

# Fast Geodesic Active Fields for Image Registration based on Splitting and Augmented Lagrangian Approaches

Dominique Zosso\*, Member, IEEE, Xavier Bresson, Jean-Philippe Thiran, Senior Member, IEEE

**Abstract**—In this paper we present an efficient numerical scheme for the recently introduced Geodesic Active Fields (GAF) framework for geometric image registration. This framework considers the registration task as a weighted minimal surface problem. Hence, the data-term and the regularization-term are combined through multiplication in a single, parametrization invariant and geometric cost functional. The multiplicative coupling provides an intrinsic, spatially varying and data-dependent tuning of the regularization strength, while the parametrization invariance allows working with images of non-flat geometry, generally defined on any smoothly parametrizable manifold. The resulting energy-minimizing flow, however, has poor numerical properties. Here, we provide an efficient numerical scheme that uses a splitting approach: data and regularity terms are optimized over two distinct deformation fields that are constrained to be equal via an augmented Lagrangian approach. Our approach is more flexible than standard Gaussian regularization, since one can interpolate freely between isotropic Gaussian and anisotropic TV-like smoothing. In this work, we compare the Geodesic Active Fields method against the popular Demons method and three more recent state-of-the-art algorithms: NL-optical flow [1], MRF image registration [2], and landmark-enhanced large displacement optical flow [3]. Overall, we can show the advantages of the proposed FastGAF method. It compares strictly favorably against Demons, both in terms of registration speed and quality. Over the range of example applications, it also consistently produces results not far from more dedicated state-of-the-art methods, illustrating the flexibility of the proposed framework.

**Index Terms**—Augmented Lagrangian, Biomedical image processing, Computational geometry, Diffusion equations, Geodesic Active Fields, Image registration, Non-convex optimization, Operator Splitting.

## I. INTRODUCTION

**I**MAGE REGISTRATION is the concept of mapping corresponding, homologous points of different images, representing a same object. In practice, however, it is often difficult to establish correspondence in images based on this definition. For automatic image registration, it is commonplace to substitute homology by a measurable criterion of image

This work is supported by the Swiss National Competence Center in Biomedical Imaging (NCCBI), the Swiss National Science Foundation (SNF) under grant PBELP2\_137727, and by Hong Kong GRF grant #110311.

J.-Ph. Thiran is with the Signal Processing Laboratory (LTS5), École Polytechnique Fédérale de Lausanne (EPFL), Station 11, CH-1015 Lausanne, Switzerland, jp.thiran@epfl.ch.

D. Zosso was with LTS5 at EPFL, and is now with the Department of Mathematics, University of California, Los Angeles (UCLA), Box 951555, Los Angeles, CA 90095-1555, USA, zosso@math.ucla.edu.

X. Bresson is with the Department of Computer Science, City University of Hong Kong, Kowloon, Hong Kong SAR, xbresson@cityu.edu.hk.

dissimilarity, which is to be minimized by an unknown deformation field  $u$ . The determination of this deformation field is an ill-posed inverse problem, and regularity constraints are usually introduced to solve it.

A multitude of approaches to solve the registration problem exist, see [4], [5], [6], [7], [8] and references therein. The most important conceptual differences are regarding similarity criterion (intensity-based, surfaces, landmarks, other features), deformation parametrization (dense/non-parametric, rigid and affine models, non-rigid models using splines, wavelets, radial or other basis functions), regularity constraints (smoothness, diffeomorphism, FEM), and optimization methods.

Here, we focus on the non-parametric variational approach, where the image distance metric and the regularization penalty are commonly incorporated into a single energy minimization model, a.k.a. variational model, e.g., [9]. The energy functionals are commonly of the general form

$$E = E_{\text{data}} + \gamma \cdot E_{\text{regularization}}, \quad \gamma > 0. \quad (1)$$

A popular algorithm of this class is called Demons [10], which is today despite its age still a commonly used method in medical image registration because of its conceptual simplicity and numerical rapidity. Modern Demons essentially consist of a two-step iterative scheme, involving an image-based data-step and a Gaussian smoothing step for regularity. Demons has two important short-comings: Gaussian convolution is only fast on Cartesian grids, and further the linear diffusion regularization might not be suitable for all registration tasks.

Therefore, in previous work [11], we have proposed a new framework called “Geodesic Active Fields” (GAF). The GAF energy belongs to the class of (weighted) minimal surface problems. In other words, the minimization flow drives the deformation field towards a harmonic map corresponding to the solution of the registration problem. To this end, the deformation field regularity is measured with the Polyakov energy [12], weighted by a suitable image distance borrowed from standard registration models.

The GAF registration method shares important properties and similarities with the well-known geodesic active contours (GAC) model [13] in image segmentation. For example, our registration method is re-parametrization invariant, like the GAC model. Further, our registration method can be designed to work on any kind of surface, such as the sphere.

While in [11] we have introduced the concept of GAF along with some prototype results for purely illustrative purposes, the main drawback was the relatively poor computational

performance, compared to state-of-the-art methods, including Demons. Here, we want to address these numerical and performance shortcomings and provide a numerical scheme that considerably improves the speed of the GAF energy minimization. The basic idea is to use splitting and an augmented Lagrangian method borrowed from optimization theory, such as [14], [15], which aims at solving some optimization problems efficiently through simpler sub-optimization problems. In our case, it consists in splitting the data term and the regularization term, which are coupled with the product operator. The splitting is then processed in an augmented Lagrangian approach to guarantee the equivalence with the original optimization problem [16]. However, we observe that the splitting method is applied to a non-convex functional (product of the data term and the regularization term) which is thus not necessarily guaranteed to converge to a global solution, even if all our experiments converged to satisfying solutions. The main interest of the proposed method is the splitting of the rather complex GAF problem into smaller sub-problems, for which fast solution schemes exist.

Here, Demons will serve as baseline for performance comparisons due to its structure very similar to GAF. This choice might appear odd at first, considering that Demons have been introduced back in 1998 [10], and that many other algorithms have since been proposed. However, despite its age, Demons is still very popular and widely used, particularly in medical imaging. Indeed, in a comparative study in 2003, Demons outperformed other methods in brain matching [17]. Today, new applications of standard and diffeomorphic Demons [18] are reported regularly, e.g. [19], [20], [21], [22], [23], [24]. Further, very fast implementations on GPU have been presented [25], [26], and new flavors and modifications of Demons are still developed, e.g. [27]. We therefore believe that the comparison of our proposed algorithm to the very closely related classical Demons method is sensible. We also note that a good part of alterations made to this classical Demons framework over the last almost 15 years can also be incorporated into the proposed GAF scheme.

Beyond, in order to compare with more recent, cutting-edge models than Demons, we also include comparisons to more specialized image registration and optical flow methods: NL-optical flow [1], MRF image registration [2], and landmark-enhanced large displacement optical flow [3].

The rest of this paper is organized as follows. First, we briefly recall the GAF framework in section II. Then, in section III we make use of a splitting scheme and augmented Lagrangians (AL) to get a fast minimization scheme for the GAF energy. We setup both, a stereo vision, an optical flow and a medical 2D registration test case, and comparisons with other methods, in section IV. Finally, we will give a short conclusion and outlook in section V.

## II. GEODESIC ACTIVE FIELDS

In this section we recall the GAF framework for image registration, introduced in [11]. The deformation field is embedded as a mapping between the  $n$ -dimensional image domain and an  $m$ -dimensional space, where  $m > n$ . This is

achieved by letting the components of the deformation field become additional dimensions of the embedding space, in close analogy to the Beltrami framework for image smoothing and restoration [28]. The embedded manifold then evolves towards a weighted minimal surface, while being attracted by a deformation field that brings the two images into registration. The main strengths of this framework are:

- 1) The flexibility to register images on any Riemannian manifold, i.e., on any smooth and parametrized surface.
- 2) The invariance under re-parametrization of the proposed energy, like the GAC energy [13] for the segmentation problem.
- 3) The data-dependent adaptation of the regularization strength thanks to the multiplicative weighting.
- 4) The ability to work with multi-scale images, where the relation between space and scale is inherently accounted for.

In the most general form, we register a pair of  $n$ -dimensional images defined on a Riemannian domain  $\Omega \subset \mathbb{R}^n$  with coordinates  $\mathbf{x} = (x_1, \dots, x_n)$ . The deformation field acts along  $p \leq n$  dimensions, i.e.,  $\mathbf{u} : \Omega \mapsto \mathbb{R}^p, \mathbf{u}(\mathbf{x}) = (u_1(\mathbf{x}), \dots, u_p(\mathbf{x}))$ . At the very core of GAF, the deformation field is seen as a surface or hypersurface embedded in a higher dimensional space, much like images embedded with the Beltrami framework [28]. On these embeddings, a Riemannian structure can be introduced: the metric  $\mathcal{G}$  locally measures the distances on the embedded deformation field, whereas in the higher dimensional embedding space distances are measured using  $\mathcal{H}$ .

The embedding  $X : \mathbb{R}^n \rightarrow \mathbb{R}^{m=n+p}$ , and the local metric tensors  $\mathcal{H} \in \mathbb{R}^{m \times m}$  and  $\mathcal{G} \in \mathbb{R}^{n \times n}$  are chosen as follows:

$$\begin{cases} X : (x_1, \dots, x_n) \rightarrow (x_1, \dots, x_n, u_1, \dots, u_p), \\ \mathcal{H}(\mathbf{x}, \mathbf{u}) \text{ is arbitrary,} \\ \mathcal{G}(\mathbf{x}, \mathbf{u}) = J^T(\mathbf{x}, \mathbf{u})\mathcal{H}(\mathbf{x}, \mathbf{u})J(\mathbf{x}, \mathbf{u}), \end{cases} \quad (2)$$

where  $x_1, \dots, x_n$  denote the spatial components of the image and  $u_1, \dots, u_p$  are the components of the dense deformation field. The  $m \times n$  matrix  $J$  denotes the Jacobian of the embedding defined by  $X$ . The manifolds associated with  $\mathcal{G}$  and  $\mathcal{H}$  are isometric i.e., the tensor  $\mathcal{G}$  of the deformation field is obtained from  $\mathcal{H}$  of the embedding space through the pullback relation. Now, we abbreviate the determinant of the deformation field's metric tensor as:

$$g(\mathbf{x}, \mathbf{u}) := \det(\mathcal{G}(\mathbf{x}, \mathbf{u})). \quad (3)$$

Based on this choice, we define the following general registration energy functional, which is a weighted Polyakov energy [29], [12], for the geodesic active fields (GAF):

$$E_{GAF}(\mathbf{u}) = \int f(\mathbf{x}, \mathbf{u}) \sqrt{g(\mathbf{x}, \mathbf{u})} \, d\mathbf{x}, \quad (4)$$

where the weighting function  $f = f(\mathbf{x}, \mathbf{u})$  is arbitrary, and represents a penalty with respect to the alignment of the two images.

Indeed, the purpose of the weighting function  $f$  is to drive the deformation field toward minimal surfaces that bring the two images into registration. Hence, the weighting function is naturally chosen to be an image distance metric, penalizing

local image mismatch. An intuitive primer for mono-modal image registration is the squared error metric [30], leading to:

$$f(\mathbf{x}, \mathbf{u}) = 1 + \alpha \cdot (\mathcal{M}(\mathbf{x} + \mathbf{u}) - \mathcal{F}(\mathbf{x}))^2, \quad (5)$$

where  $\mathcal{F}$  and  $\mathcal{M}$  refer to the fix and moving images, respectively. In other cases, e.g., for stereo vision, the absolute error norm might be more appropriate:

$$f(\mathbf{x}, \mathbf{u}) = 1 + \alpha \cdot |\mathcal{M}(\mathbf{x} + \mathbf{u}) - \mathcal{F}(\mathbf{x})|. \quad (6)$$

For other examples such as multimodal image registration, or more sophisticated deformation models, refer to [31].

As we work with sampled images and deformation fields, we adapt the notation of variables and the energy accordingly. First, let  $\mathbf{x} \in \mathbb{R}^{N \times n}$  denote the matrix containing the coordinates of all samples, where  $N$  is the number of spatial samples, and where  $n$  is the dimension of the images. Pixel  $i$  is located at  $\mathbf{x}_i \in \mathbb{R}^n$ . Similarly,  $\mathbf{u}_i = \mathbf{u}(\mathbf{x}_i) \in \mathbb{R}^p$  is the deformation vector at  $\mathbf{x}_i$ . For any  $i \in [1, N]$  let us write  $x_{i,j}$ ,  $j \in [1, n]$  and  $u_{i,q}$ ,  $q \in [1, p]$  to denote a specific component of those vectors. Finally, the weighting function and the square root of the metric tensor are rewritten as column vectors,  $F, G \in \mathbb{R}^N$ , respectively:

$$F_i = f(\mathbf{x}_i, \mathbf{u}_i) \quad \forall i \in [1, N], \quad (7)$$

$$G_i = \sqrt{g(\mathbf{x}_i, \mathbf{u})} \quad \forall i \in [1, N]. \quad (8)$$

This allows rewriting the GAF energy in terms of a standard vectorial inner product:

$$E_{GAF} = \langle F, G \rangle = \sum_{i=1}^N F_i G_i = F^T G. \quad (9)$$

In summary, the notation changes as follows:

$$\begin{aligned} \mathbf{x} \in \Omega \subset \mathbb{R}^n &\rightarrow \mathbf{x} \in \mathbb{R}^{N \times n} \\ \mathbf{u}(\mathbf{x}) \in \mathbb{R}^p &\rightarrow \mathbf{u}(\mathbf{x}) \in \mathbb{R}^{N \times p} \\ f(\mathbf{x}, \mathbf{u}) \in \mathbb{R}^+ &\rightarrow F(\mathbf{x}, \mathbf{u}) \in \mathbb{R}^{+N} \\ \sqrt{g(\mathbf{x}, \mathbf{u})} \in \mathbb{R}^+ &\rightarrow G(\mathbf{x}, \mathbf{u}) \in \mathbb{R}^{+N} \\ E_{GAF}(\mathbf{u}) = \int_{\Omega} f \sqrt{g} d\mathbf{x} &\rightarrow E_{GAF}(\mathbf{u}) = F^T G. \end{aligned} \quad (10)$$

### III. FASTGAF ENERGY MINIMIZATION

The preliminary results presented in [11] were based on a direct implementation of the flow (4), using a simple forward Euler scheme. Here, we speed up the optimization task with a splitting approach, that minimizes the weighting function and the metric tensor term of the GAF energy separately, tightly coupled through an augmented Lagrangian (AL) method.

Lagrangian multiplier methods are a powerful and commonly used technique for constrained optimization. They are known to outperform ordinary penalty methods – where the constraint is only encouraged but not enforced [32], [16]. Indeed, a combination of both ordinary penalty and Lagrangian multiplier terms in the energy functional leads to the so-called Augmented Lagrangian (AL), that exhibits better convergence properties [14], [16]. Several recent, successful TV-regularized image processing problems, such as [33], [34], can be derived from such an AL scheme.

#### A. Splitting

First, we note that in GAF, the unknown  $\mathbf{u} \in \mathbb{R}^{N \times p}$  is a matrix of size  $N \times p$ , where  $p$  is the co-dimension of the deformation field, i.e., the number of associated deformation field components. As first step, we transform the unconstrained GAF energy minimization problem over one deformation field  $\mathbf{u}$ :

$$\min_{\mathbf{u}} \{E_{GAF} = F(\mathbf{u})^T G(\mathbf{u})\} \quad (11)$$

into an equivalent, constrained minimization problem on two coupled deformation fields  $\mathbf{u}$  and  $\mathbf{v}$ :

$$\min_{\mathbf{u}, \mathbf{v}} \{E_{GAF} = F(\mathbf{u})^T G(\mathbf{v})\} \quad s.t. \quad \mathbf{u} = \mathbf{v}. \quad (12)$$

We can obtain an unconstrained minimization problem and guarantee to satisfy the linear constraint  $\mathbf{u} = \mathbf{v}$  using the following AL scheme [14], [16]:

$$AL(\mathbf{u}, \mathbf{v}, \boldsymbol{\lambda}) := F(\mathbf{u})^T G(\mathbf{v}) + \langle \boldsymbol{\lambda}, \mathbf{u} - \mathbf{v} \rangle_{N,p} + \frac{r}{2} \|\mathbf{u} - \mathbf{v}\|_F^2, \quad (13)$$

where  $\boldsymbol{\lambda} \in \mathbb{R}^{N \times p}$  is the Lagrangian multiplier matrix, in the same space as  $\mathbf{u}$  and  $\mathbf{v}$ ,  $\langle \boldsymbol{\lambda}, \mathbf{u} - \mathbf{v} \rangle_{N,p} = \sum_{i=1}^N \sum_{d=1}^p \lambda_{i,d} (u_{i,d} - v_{i,d})$  is the scalar product between two matrices of the same dimension  $N \times p$ , and where  $\|M\|_F^2 = \sum_{i,j} m_{i,j}^2$  is the square of the Matrix Frobenius norm. From now on,  $r > 0$  is a positive constant; how to choose it will be discussed later in section IV-F.

The constrained minimization problem is then solved by looking for a saddle point of the associated AL. To this end, the minimization w.r.t.  $\mathbf{u}$  and  $\mathbf{v}$  can be carried out separately, followed by a dual ascent step (Lagrangian multiplier update). We get the following split optimization scheme:

$$\begin{cases} \mathbf{u}^{k+1} = \operatorname{argmin}_{\mathbf{u}} \{F(\mathbf{u})^T G(\mathbf{v}^k) \\ \quad + \langle \boldsymbol{\lambda}^k, \mathbf{u} - \mathbf{v}^k \rangle_{N,p} + \frac{r}{2} \|\mathbf{u} - \mathbf{v}^k\|_F^2\}, \\ \mathbf{v}^{k+1} = \operatorname{argmin}_{\mathbf{v}} \{F(\mathbf{u}^{k+1})^T G(\mathbf{v}) \\ \quad + \langle \boldsymbol{\lambda}^k, \mathbf{u}^{k+1} - \mathbf{v} \rangle_{N,p} + \frac{r}{2} \|\mathbf{u}^{k+1} - \mathbf{v}\|_F^2\}, \\ \boldsymbol{\lambda}^{k+1} = \boldsymbol{\lambda}^k + r(\mathbf{u}^{k+1} - \mathbf{v}^{k+1}). \end{cases} \quad (14)$$

In the next paragraphs, we will present how the two respective subminimization problems can be tackled efficiently.

#### B. Subminimization w.r.t. $\mathbf{u}$

The first subminimization problem in (14) deals with the partial optimization of the sub-problem w.r.t. deformation field  $\mathbf{u}$  used in the weighting function  $F(\mathbf{u})$ , i.e., the image distance function, while keeping the regularization term  $G(\mathbf{v}^k)$  fixed:

$$E_1(\mathbf{u}) := F(\mathbf{u})^T G(\mathbf{v}^k) + \langle \boldsymbol{\lambda}^k, \mathbf{u} - \mathbf{v}^k \rangle_{N,p} + \frac{r}{2} \|\mathbf{u} - \mathbf{v}^k\|_F^2. \quad (15)$$

To simplify things, we linearize  $F$  around the current estimate  $F(\mathbf{u}^k)$ . The functional derivative w.r.t.  $\mathbf{u}$  is then obtained as:

$$D_{\mathbf{u}} E_1(\mathbf{u}) = \operatorname{diag}(G(\mathbf{v}^k)) \cdot \frac{\partial F}{\partial \mathbf{u}}(\mathbf{u}^k) + \boldsymbol{\lambda}^k + r\mathbf{u} - r\mathbf{v}^k. \quad (16)$$

From the optimality condition,  $D_{\mathbf{u}}E_1(\mathbf{u}) = 0$ , we get the update equation directly:

$$\mathbf{u}^{k+1} = \mathbf{v}^k - \frac{1}{r} \left( \boldsymbol{\lambda}^k + \text{diag}(G(\mathbf{v}^k)) \cdot \frac{\partial F}{\partial \mathbf{u}}(\mathbf{u}^k) \right). \quad (17)$$

The stability of this step is limited by the constant  $r$ : a small  $r$  results in a wider step away from the current estimate, and consequently the linear approximation of the image might not be good enough. We present a solution in the next paragraph.

### C. Balancing the computational complexity

The first order approximation requires small step sizes, i.e. big  $r$ . Further, as we will see below, the exact inverse solution of the second problem is computationally more challenging, but stable irrespective of the step size  $r$ . Therefore, our goal is to both balance the computational complexity between the two tasks, and alleviate the step size restrictions in the first task. Here we propose a fixed-point scheme to address these limitations. First, let us introduce a virtual time  $t$  and define a corresponding gradient descent equation associated to the functional derivative (parabolic problem), instead of solving directly for the linearized optimality condition (elliptic problem):

$$\frac{\partial \mathbf{u}}{\partial t} = -D_{\mathbf{u}}E_1(\mathbf{u}). \quad (18)$$

We discretize in time using a semi-implicit scheme:

$$\frac{\mathbf{u}^{n+1} - \mathbf{u}^n}{\tau} = -\text{diag}(G(\mathbf{v}^k)) \cdot \frac{\partial F}{\partial \mathbf{u}}(\mathbf{u}^n) - \boldsymbol{\lambda}^k - r\mathbf{u}^{n+1} + r\mathbf{v}^k. \quad (19)$$

Using  $\mathbf{u}^{n=0} := \mathbf{u}^k$  as initial condition, we iterate the scheme

$$\mathbf{u}^{n+1} = \frac{\mathbf{u}^n - \tau \text{diag}(G(\mathbf{v}^k)) \cdot \frac{\partial F}{\partial \mathbf{u}}(\mathbf{u}^n) - \tau \boldsymbol{\lambda}^k + \tau r \mathbf{v}^k}{1 + \tau r} \quad (20)$$

until convergence towards a fixed point such that  $\mathbf{u}^{k+1} := \mathbf{u}^{n \rightarrow \infty}$ . We choose  $\tau = \frac{1}{Lr}$ ,  $L \in \mathbb{N}$ . This choice corresponds to a gradient-descent step-size,  $\tau/(1+\tau r) = 1/(L+1)r$ , which is shorter than the direct solution step  $1/r$  to the elliptic problem (17) by a factor  $(L+1)$ . To balance this, in practice, roughly  $2L$  iterations are enough to achieve a satisfying convergence. The benefit of this iterated optimization is increased accuracy regarding the data-term optimization (if we keep the same  $r$ ), or faster overall convergence in terms of outer optimization iterations, thereby using less regularization steps (if  $r$  is decreased by a factor up to  $(L+1)$ ).

### D. Subminimization w.r.t. $\mathbf{v}$

The second subminimization problem in (14) deals with the optimization of the deformation field in terms of the regularizer  $G(\mathbf{v})$ , while, this time, keeping the weighting function term  $F(\mathbf{u}^{k+1})$  fixed:

$$E_2(\mathbf{v}) := F(\mathbf{u}^{k+1})^T G(\mathbf{v}) + \langle \boldsymbol{\lambda}^k, \mathbf{u}^{k+1} - \mathbf{v} \rangle_{N,p} + \frac{r}{2} \|\mathbf{u}^{k+1} - \mathbf{v}\|_F^2. \quad (21)$$

The derivative of the first term with respect to the deformation field  $\mathbf{v}$  contains both the weighted Laplace-Beltrami operator and a term involving the weighting function's spatial gradient. We discard the latter term since the weighting function's

spatial gradient mainly reflects the noise in image acquisitions. The remaining weighted Laplace-Beltrami operator is a “div-grad”-operator affected by the metric  $\mathcal{G}$ , thus rendering the smoothing diffusion anisotropic. To discretize, we use a second order central differences standard scheme, as in [35]. First, we simplify the notation and shorten the expression of the anisotropy tensor:

$$\begin{pmatrix} a & b \\ b & c \end{pmatrix}_i = \sqrt{g(\mathbf{x}_i, \mathbf{u})} \mathcal{G}^{-1}(\mathbf{x}_i, \mathbf{u}). \quad (22)$$

Now, we introduce the Laplacian-like matrix  $W \in \mathbb{R}^{N \times N}$ :

$$W_{i,j} = 2\beta^2 \cdot \begin{cases} -a(i) - c(i) & j = i \\ -\frac{1}{2}(a(i+1,0) + a(i-1,0)) & j = i_{\pm 1,0} \\ -\frac{1}{2}(c(i_{0,+1}) + c(i_{0,-1})) & j = i_{0,\pm 1} \\ \frac{1}{2}(a(i) + a(j)) & j = i_{\pm 1} \\ \frac{1}{2}(c(i) + c(j)) & j = i_{0,\pm 1} \\ \frac{(b(i_{\pm 1,0}) + b(i_{0,\pm 1}))}{4} & j = i_{\pm 1,\pm 1} \\ \frac{-(b(i_{\pm 1,0}) + b(i_{0,\mp 1}))}{4} & j = i_{\pm 1,\mp 1} \\ 0 & \text{otherwise,} \end{cases} \quad (23)$$

where  $i_{\pm 1,0} \mapsto (m \pm 1, n)$  denotes the index of the east/west neighbor of pixel  $i \mapsto (m, n)$ , and  $i_{0,\pm 1} \mapsto (m, n \pm 1)$  denotes the index of the south/north neighbor, respectively. Finally, having omitted the term in  $D_{\mathbf{x}}F$ , we may write

$$\frac{\partial F(\mathbf{u}^{k+1})^T G(\mathbf{v})}{\partial \mathbf{v}} \approx -\text{diag}(F(\mathbf{u}^{k+1})) \cdot W \mathbf{v}. \quad (24)$$

Overall, we consider the following approximation to the complete functional derivative corresponding to  $E_2$ :

$$D_{\mathbf{v}}E_2(\mathbf{v}) = -\text{diag}(F(\mathbf{u}^{k+1})) \cdot W \mathbf{v} - \boldsymbol{\lambda}^k - r(\mathbf{u}^{k+1} - \mathbf{v}) \quad (25)$$

and, by the optimality condition again, we directly solve for the update:

$$\mathbf{v}^{k+1} = \left( I - \frac{1}{r} \text{diag}(F(\mathbf{u}^{k+1})) \cdot W \right)^{-1} \left( \mathbf{u}^{k+1} + \frac{1}{r} \boldsymbol{\lambda}^k \right). \quad (26)$$

Since we are only interested in the solution of this linear system, it is not necessary to explicitly compute the inverse of the right-hand-side matrix. Instead, more sophisticated solvers can exploit the sparsity of the system. We call this scheme the *exact inverse FastGAF*, in contrast to the approximate inverse FastGAF that will be introduced below. Note that this scheme highly resembles a semi-implicit Euler diffusion scheme, and therefore it can be considered unconditionally stable w.r.t.  $r$  [36].

### E. A Jacobi scheme for approximate inversion

Instead of an exact computation of the update (26), which is computationally expensive, we propose to use an iterative Jacobi scheme as an approximation, see e.g., [37]. Therefore, let us decompose the system matrix in a diagonal  $D$  and a remainder matrix  $R$ :

$$D + R = \left( I - \frac{1}{r} \text{diag}(F(\mathbf{u}^{k+1})) \cdot W \right), \quad (27)$$

where  $D$  and  $R$  can be given explicitly:

$$\begin{aligned} D_{ii} = 1 + \frac{2\beta^2 F_i}{r} (a(i) + c(i)) \\ + \frac{\beta^2 F_i}{r} (a(i_{+1,0}) + a(i_{-1,0})) \\ + \frac{\beta^2 F_i}{r} (c(i_{0,+1}) + c(i_{0,-1})) \end{aligned} \quad (28)$$

and

$$R_{ij} = \begin{cases} -\frac{\beta^2 F_i}{r} (a(i) + a(j)) & j = i_{\pm 1,0} \\ -\frac{\beta^2 F_i}{r} (c(i) + c(j)) & j = i_{0,\pm 1} \\ -\frac{\beta^2 F_i (b(i_{\pm 1,0}) + b(i_{0,\pm 1}))}{4} & j = i_{\pm 1,\pm 1} \\ \frac{\beta^2 F_i (b(i_{\pm 1,0}) + b(i_{0,\mp 1}))}{4} & j = i_{\pm 1,\mp 1} \\ 0 & \text{otherwise.} \end{cases} \quad (29)$$

Let us denote the right hand term  $\mathbf{b} = (\mathbf{u}^{k+1} + \frac{1}{r}\boldsymbol{\lambda}^k)$ . Now, the Jacobi scheme approximates  $\mathbf{v}^{k+1}$  as a fixed point solution, with  $\mathbf{v}^{k+\frac{0}{J}} = \mathbf{u}^{k+1}$  as possible initialization:

$$(D + R)\mathbf{v} = \mathbf{b} \quad (30)$$

$$\mathbf{v}^{k+\frac{j}{J}} = D^{-1} \left( \mathbf{b} - R\mathbf{v}^{k+\frac{j-1}{J}} \right), \quad j = 1, \dots, J, \quad (31)$$

where  $D^{-1}$  is straightforward to compute, and where convergence can be guaranteed since  $W$  is definite positive.

The complete *approximate inverse FastGAF* energy minimization scheme is summarized in algorithm 1.

#### Algorithm 1 Approximate-inverse FastGAF algorithm

1: Initialize  $\mathbf{u}^0$ ,  $\mathbf{v}^0$  and  $\boldsymbol{\lambda}^0$ .

2: **repeat**

$$\begin{cases} \mathbf{u}^{k+\frac{l+1}{2L}} = \frac{\mathbf{u}^{k+\frac{l}{2L}} - \frac{1}{Lr} \text{diag}(G(\mathbf{v}^k)) \cdot \frac{\partial F}{\partial \mathbf{u}}(\mathbf{u}^{k+\frac{l}{2L}}) - \boldsymbol{\lambda}^k + r\mathbf{v}^k}{1 + \tau r} \\ l = 0 \dots (2L - 1) \\ \\ \mathbf{v}^{k+\frac{j}{J}} = \begin{cases} D^{-1} \left( \mathbf{u}^{k+1} + \frac{1}{r}\boldsymbol{\lambda}^k - R\mathbf{u}^{k+1} \right) & j = 1 \\ D^{-1} \left( \mathbf{u}^{k+1} + \frac{1}{r}\boldsymbol{\lambda}^k - R\mathbf{v}^{k+\frac{j-1}{J}} \right) & j = 2 \dots J \end{cases} \\ \\ \boldsymbol{\lambda}^{k+1} = \boldsymbol{\lambda}^k + r(\mathbf{u}^{k+1} - \mathbf{v}^{k+1}) \end{cases} \quad (32)$$

3: **until** convergence.

#### IV. EXPERIMENTS

We test the FastGAF scheme on three example applications: stereo vision disparity recovery, small displacement optical flow, and large displacement 2D registration on a brain MRI slice. The results of the proposed FastGAF algorithm are compared to the popular Demons algorithm baseline, as well as three more recent, state-of-the-art optical flow/image registration methods: Sun et al. “non-locally regularized optical flow” [1], Glocker et al. “MRF image registration” [2], and Brox

et al. “large displacement optical flow” [3]. These three state-of-the-art methods have their code and/or binaries publicly available. We measure endpoint error EPE (in pixels) and percentage of wrong pixels  $w_1$  i.e., rate of pixels off by more than 1 pixel,  $w_2$  (off by more than 2 pixels), and angular error AE (where applicable) [38] as registration quality indicators.

In addition, to illustrate the geometrical flexibility of the proposed FastGAF scheme, we show the results of a hemispherical toy-registration problem.

#### A. Stereo vision

An example of stereo vision depth recovery problem is shown in Fig. 1. The image pair `tsukuba` is a well known test image, taken from the middlebury benchmark set for stereo vision [39]. We are aware of the existence of a broad variety of high performance algorithms for the stereo vision depth recovery problem. Neither Demons, nor our proposed method are particularly well suited to compete with those state-of-the-art stereo vision methods. Here, we simply explore the stereo vision problem as an illustrative example due to its relatively simple embedding.

Indeed, a fundamental assumption in classical stereo depth recovery is the simple epipolar geometry relating the two images in the pair. Photos are acquired on a common image plane and cameras are shifted horizontally. Therefore, corresponding points in the image pair lie on the same horizontal line. The (relative) amount of horizontal shift between corresponding pixels is then a measure of depth in the 3D scene.

Consequently, the co-dimension of the deformation field is reduced to  $p = 1$ , while  $n = 2$  for 2D images, which results in a very accessible case of GAF embedding:

$$\begin{cases} X : (x, y) \rightarrow (x, y, u) \\ \mathcal{H} = \text{diag}(1, 1, \beta^2) \\ \mathcal{G} = \begin{bmatrix} 1 + \beta^2 u_x^2 & \beta^2 u_x u_y \\ \beta^2 u_x u_y & 1 + \beta^2 u_y^2 \end{bmatrix} \\ g = 1 + \beta^2 |\nabla u|^2. \end{cases} \quad (33)$$

Put into the general equations we get the following energy functional:

$$E_{GAF}(\mathbf{u}) = \int f \sqrt{1 + \beta^2 |\nabla u|^2} dx dy. \quad (34)$$

Results are illustrated in Fig. 1 and metrics reported in table I. The ranking of methods is very difficult, since Sun et al. has the lowest  $w_1$ , the proposed FastGAF yields lowest  $w_2$ , and Brox et al. suffer from lowest EPE.

#### B. 2D optical flow

The second example, `rubberwhale`, is a test image pair frequently used in optical flow benchmarking. The ground truth deformation is fairly small and essentially piece-wise smooth. Deformation takes place along both image dimensions.

The test image pair and results are illustrated in Fig. 2, numbers are again reported in table I. In summary, here Sun et al. performs best in all quality metrics, while Brox et al. and the proposed FastGAF method come in second and third, closely together.

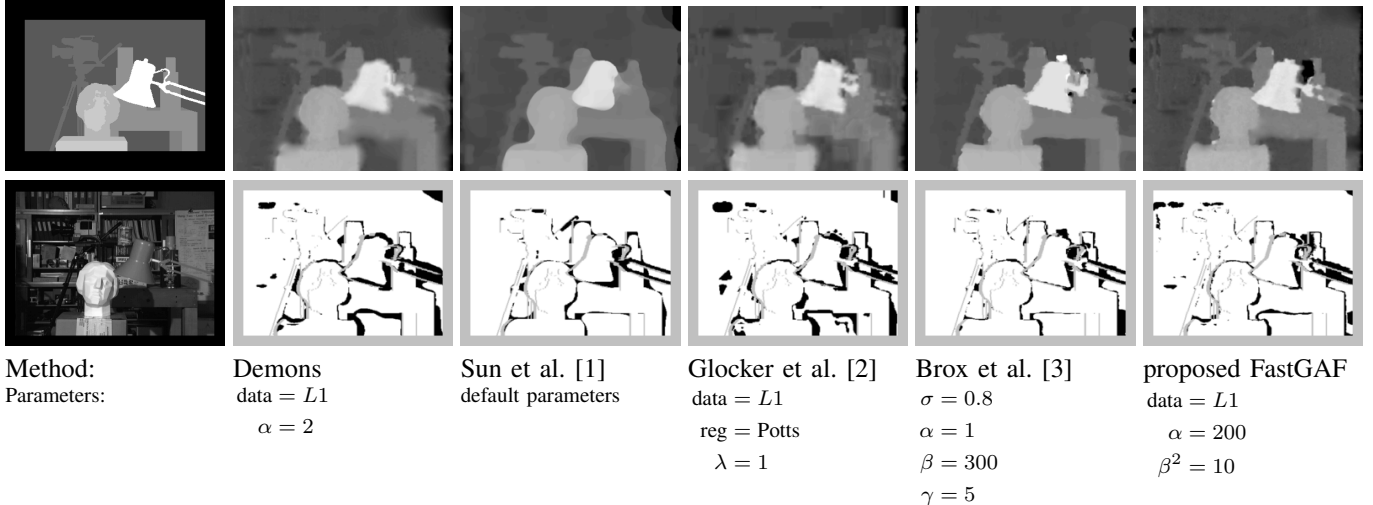


Fig. 1: Results of the stereo-vision depth-recovery problem (tsukuba). Top row: Ground truth depth map and disparities recovered by the 5 evaluated methods. Bottom row: One of the input frames, and the 5 different error maps. Grey pixels are not considered (no ground truth, or expected occlusion), black pixels indicate error (recovered disparity more than one pixel off).

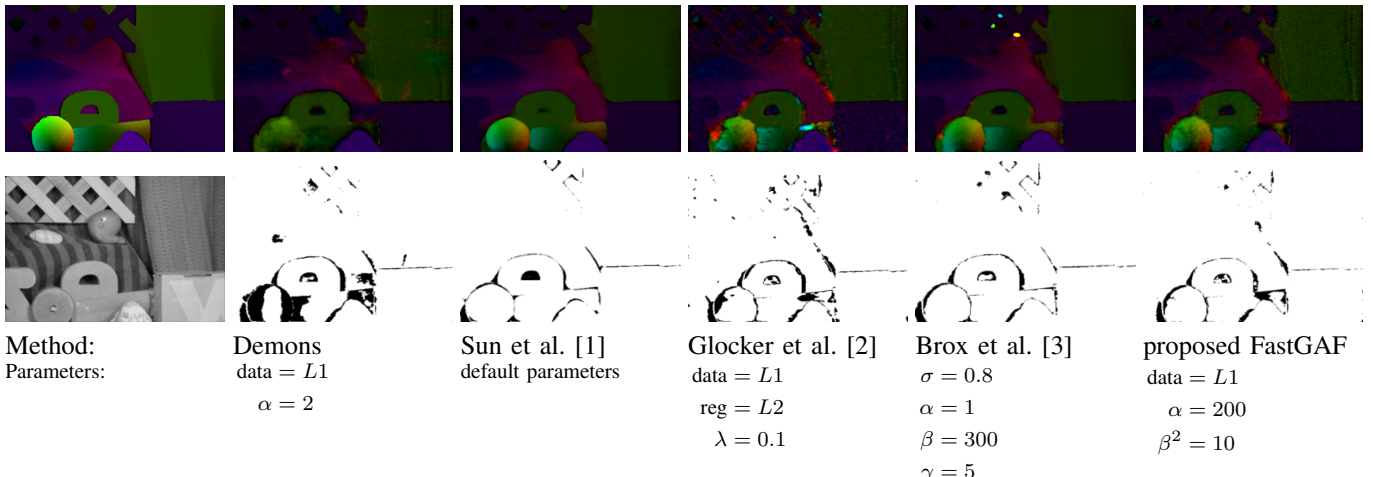


Fig. 2: Results of the optical flow experiment (rubberwhale). Top row: Ground truth (leftmost) and recovered flow fields (color codes direction, intensity codes amplitude). Bottom row: One frame of the input pair (leftmost) and the 5 respective error maps (black pixels are more than one pixel off).

### C. 2D medical image registration

The third case deals with 2D registration of a highly misaligned mono-modal medical image pair. An axial slice through a T1 MRI volume is heavily deformed by a given 2D deformation field. The initial average endpoint error is 7.3 pixels. The images have a resolution of  $317 \times 317$  pixels and are both affected by 5% additive Gaussian noise.

The test images as well as the obtained results are shown in Fig. 3, while numbers are found in table I. Here, Glocker et al. is the winner, while the proposed FastGAF comes in second, with quite some margin to the other methods.

### D. Ranking of methods

We base our assessment of performance of the 5 different methods on the results reported in table I. One quickly realizes

that there seems not to be an immediate winning method: in the stereo case, results are very heterogeneous between different quality measures. The optical flow case is clearly won by NL-optical flow [1], whereas the 2D medical image registration task is best solved by MRF-based registration [2], immediately followed by the proposed FastGAF method.

In order to summarize, we ranked the 5 methods in all 11 quality columns independently, and aggregate the rank-sum per method ( $\sum \#$ ). The computation time is ignored here, since the 5 different methods are implemented in very different environments (Matlab, Matlab+MEX, binary only with GUI). It turns out that three methods achieve almost identical rank-sum: Sun et al. (27), Brox et al. (26), and the proposed FastGAF (27). Glocker et al. (35) comes in 4th, and Demons (50) is clearly the worst method considered. Interestingly, the proposed FastGAF method is highly ranked thanks to

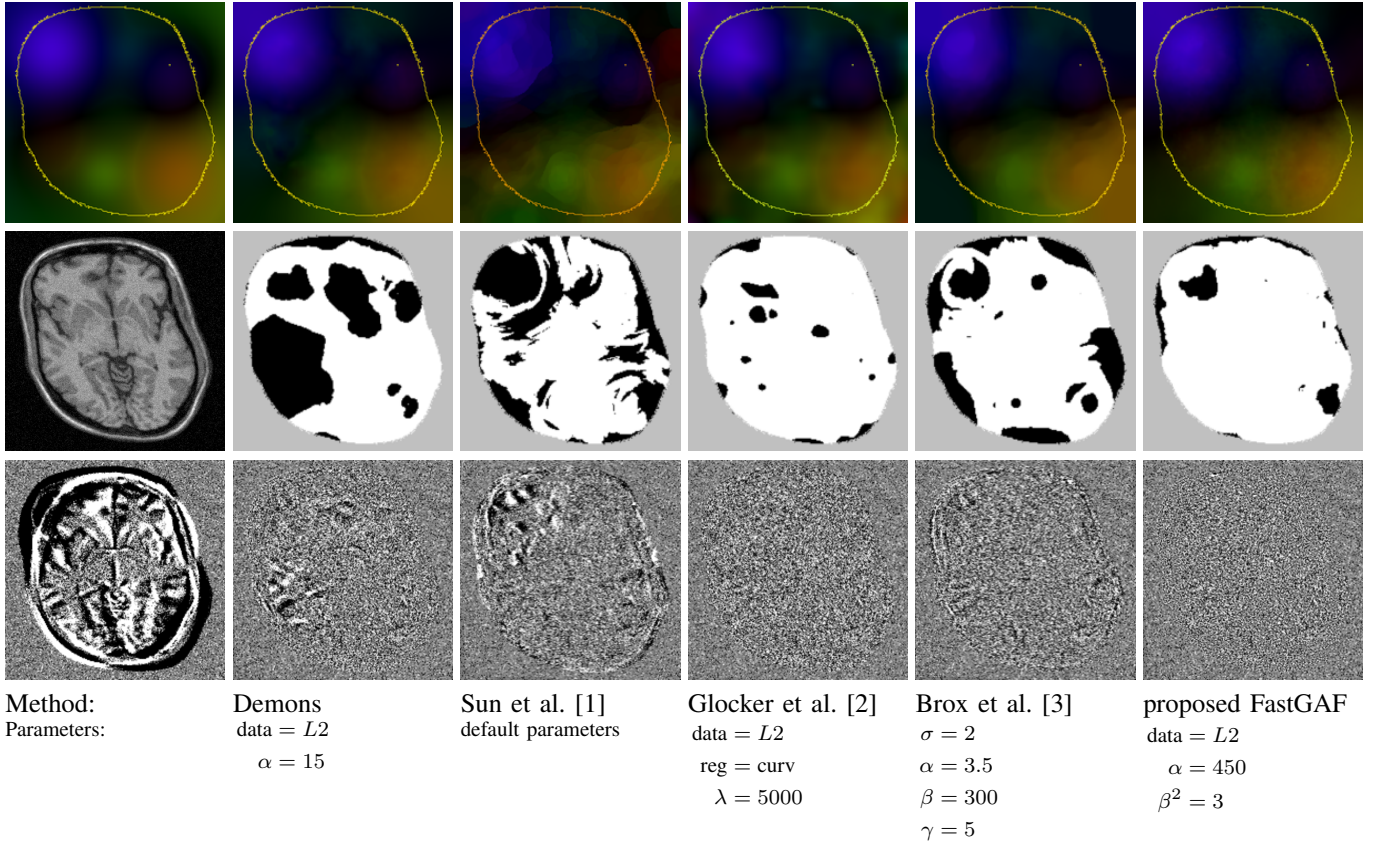


Fig. 3: Results of the medical 2D registration problem. Top row: Ground truth (leftmost) and recovered deformation fields (color codes direction, intensity codes amplitude). The yellow contour indicates the boundaries of the error evaluation mask—outside this boundary, the target frame has no intrinsic information but only noise, and we do not evaluate registration errors, there. Middle row: Target image (leftmost), and the 5 error maps (black pixels are off by more than one pixel from ground truth). Bottom row: frame difference before registration (leftmost), and the 5 frame differences after registration.

its consistent quality—it's never the best method, but always a good choice, whereas the other methods seem to work particularly good for some cases but fail for others.

To get a more quantitative comparison, we perform a paired sign-test between each pair of methods, where each different quality measurement produces a pair of samples. This is a test of the null hypothesis that performance differences between two methods come from a continuous distribution with zero median, against the alternative that the distribution does not have zero median (i.e. the performance differences are systematic). The resulting p-values for each combination are provided in table II, both ignoring and considering the computation times. The p-values confirm, that under the considered statistical test, there is no clear winner, but Demons is the clear loser. In particular, the proposed FastGAF method performs better than Demons, Glocker and Brox, but worse than Sun—however, only the difference to Demons is statistically significant.

#### E. Hemi-spherical registration

One of the main strengths of the Geodesic Active Fields method for image registration, is its intrinsic ability to deal with non-Euclidean images. Here we show an example of

a spherical image, parametrized through stereographic projection. While we use the well-known topography of the Earth as a toy example, realistic applications can be found in omni-directional vision e.g., [40]. Indeed, in [41], [42] it was shown, that a sensor image of a catadioptric camera—i.e. using spherical, paraboloid or hyperboloid mirror—is equivalent to a stereographic projection of the spherical plenoptic function.

The metric of the stereographic projection is conformal to the regular Euclidean metric [43]. The choice of the metric  $\mathcal{H}$  of the embedding space is immediate:

$$\mathcal{H} = \frac{4}{1 + x^2 + y^2} \text{diag}(1, 1, \beta^2, \beta^2). \quad (35)$$

Three typical stereographic projections—polar, equatorial and oblique—are sketched in Fig. 4(a)–(c). Here we chose an oblique projection of the Earth's topographical map for the sake of generality. The map is artificially deformed and successfully restored through registration, see Fig. 4(d)–(f).

#### F. The roles of the parameters $r$ , $L$ and $J$

The approximate-inverse FastGAF scheme introduces three new parameters to the problem. Here we want to illustrate and discuss their respective role in the optimization framework from a performance-based point of view. The images are low-

TABLE I: Computation time and quality measurements. Demons clearly comes in last and Glocker performs medium, while Sun, Brox and the proposed FastGAF method perform equally good overall.

	$\Sigma\#$	Stereo				Optical flow						Medical				
		$t$ [s]	$w_1$ [%]	$w_2$ [%]	EPE [1]	$t$ [s]	$w_1$ [%]	$w_2$ [%]	EPE [1]	AE [°]	$t$ [s]	$w_1$ [%]	$w_2$ [%]	EPE [1]	AE [°]	
Demons	50	476	10.5(4)	5.3(5)	0.5(3)	555	6.9(5)	1.2(4)	0.3(5)	10.7(5)	485	38.0(5)	17.2(5)	1.3(5)	0.5(4)	
Sun [1]	27	37	<b>6.7</b> (1)	5.0(3)	0.5(2)	35	<b>2.1</b> (1)	<b>0.3</b> (1)	<b>0.1</b> (1)	<b>4.1</b> (1)	12	33.4(4)	14.7(4)	1.1(4)	0.5(5)	
Glocker [2]	35	66	11.1(5)	5.3(4)	0.6(5)	33	4.6(4)	1.3(5)	0.3(4)	9.6(4)	25	<b>6.0</b> (1)	<b>0.2</b> (1)	<b>0.4</b> (1)	<b>0.3</b> (1)	
Brox [3]	26	45	6.7(2)	4.4(2)	<b>0.4</b> (1)	41	2.6(2)	0.5(3)	0.2(2)	5.1(2)	17	23.4(3)	8.6(3)	0.8(3)	0.5(3)	
FastGAF	27	222	7.9(3)	<b>4.0</b> (1)	0.5(4)	293	3.1(3)	0.4(2)	0.2(3)	8.1(3)	174	7.9(2)	1.2(2)	0.5(2)	0.3(2)	

Computation time  $t$  in seconds, percentages of pixels off by more than 1(2) pixels  $w_1(w_2)$ , endpoint error EPE, and angular error AE. In each column, the best result is shown in boldface. (1)–(5) are the ranks of the individual performance measurements prior to rounding (within each column). The computation time is given for the sake of completeness, but not considered in the ranking, due to the different implementation environments of the methods.  $\sum\#$  is the row-wise rank sum per method based on the individual ranks.

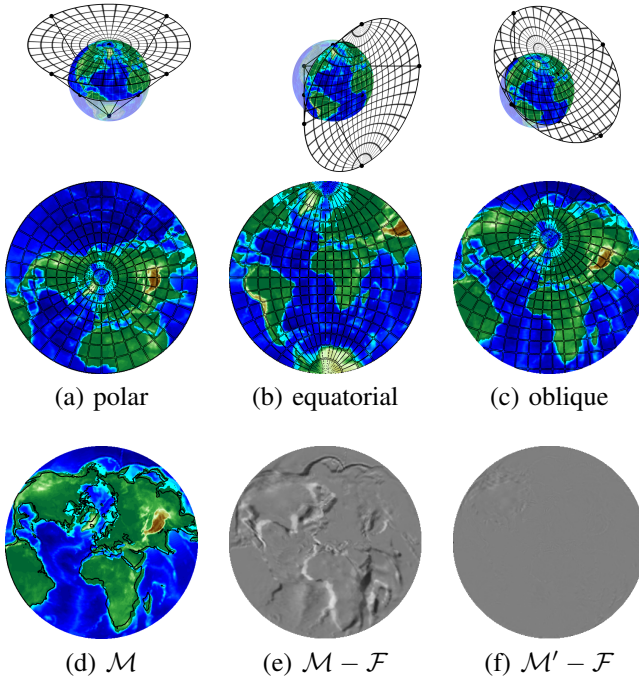


Fig. 4: (a)–(c) Different stereographic projections of the sphere. (d) Chosen oblique projection and artificial deformation (original coastlines in black). (e)–(f) Intensity differences before and after registration.

pass filtered and subsampled at different resolutions and the minimization is executed in multiple stages. In the image pyramid, each level stops after a pre-definite number of iterations  $K$ . To measure the convergence speed of the different methods, we launch registration for a whole range of different numbers of iterations  $K$ , and plot the obtained respective quality measures against the wall clock time  $t$  required.

1) *Penalty weight r*: The first novel parameter introduced with the augmented Lagrangian scheme is the penalty weight  $r$ . The penalty term is supposed to stabilize the minimization problem. Indeed, it introduces a quadratic energy on the distance between the separate split deformation fields and acts as a “leash” between the two, its elasticity being governed by  $r$ .

TABLE II: Paired sign-test of the performance measurements between methods from table I. Demons clearly loses, while all other differences are not statistically significant. Even considering computation time, FastGAF performs not significantly worse than the state-of-the-art methods.

		p-values			
		Ignoring computation time			
	Demons	Sun	Glocker	Brox	
FastGAF	> <b>0.02</b>	$\leq 1$	$\geq 0.5$	$\geq 1$	
Brox	> <b>0.003</b>	$\geq 1$	$\geq 0.5$		
Glocker	$\geq 0.2$	$\leq 0.5$			
Sun	> <b>0.02</b>				

		Considering computation time			
		Demons	Sun	Glocker	Brox
FastGAF	> <b>0.003</b>	$\leq 0.4$	$= 1$		$\leq 0.8$
Brox	> <b>0.0005</b>	$\leq 0.8$	$\geq 0.4$		
Glocker	$\geq 0.06$	$\leq 0.4$			
Sun	> <b>0.003</b>				

Read: FastGAF outperforms Demons ( $>$ ,  $p$ -value = 0.02); We reject the null hypothesis of zero-median measurement differences in a two-sided paired sign-test ( $\alpha = 0.05$ ). Or: FastGAF performs equal to or slightly worse than Sun ( $\leq$ ,  $p$ -value = 1); The null hypothesis of zero-median measurement differences in a two-sided paired sign-test cannot be rejected ( $\alpha = 0.05$ ).

The bigger this parameter, the closer  $u$  and  $v$  are tied together and the less they can diverge at each iteration. This reduces the lag between  $u$  and  $v$  and is the only way to restrict the step size at each iteration. The step size limitation is critical with respect to the data term, as due to the complexity of the images under consideration, the linear approximation of the weighting function only holds within a close vicinity of the current configuration. The impact of  $r$  on the registration performance is illustrated in fig. 5. It becomes clear, that below a certain level the optimization is unstable with respect to the data term, whereas above a certain threshold only the speed of the algorithm is affected. In particular, it becomes obvious that the penalty term itself is vital for stability, and a pure Lagrangian

approach implies severe convergence issues. In contrast, the Lagrangian multiplier is not an absolute requirement for the split GAF iterations to converge, as illustrated in fig. 5b). However, as can be seen from the charts, it improves the convergence of the algorithm especially for low penalty weight and thus confirms to be of true interest, considering its little computational extra effort.

2) *Data-step sub-iterations L*: In order to overcome the small-step requirement of the data-term, we propose to carry out several data-step optimizations within a fixed-point scheme before doing a more important smoothing step. The number of data-term optimizations per regularity-term optimization is governed by the parameter  $L$ . At  $r$  fixed, the image distance term is optimized more precisely, while by replacing  $r \leftarrow r/L$ , the leash length can be extended at the same image distance precision, thus reducing the number of smoothing steps required. This speed gain is illustrated in fig. 6. In particular with the exact-inverse FastGAF scheme, this parameter can be seen as a way of balancing the computational load between both optimization subtasks, to gain in efficiency.

3) *Regularity-step Jacobi iterations J*: In the approximate-inverse FastGAF scheme, finally, we replace the costly full inversion of the diffusion matrix by an approximating Jacobi scheme. There, the number of Jacobi iterations is given by  $J$ , controlling the desired precision of the approximate inverse. While the exact inverse has full support (full matrix), now the support of the smoothing stencil is of size  $2J + 1$  in each dimension and the speedup is obviously considerable. Close to the critical step-length  $r$ , however, the algorithm does not properly converge for small, in particular odd,  $J$ . Beyond, the speedup comes at little loss of precision, which is reasonable since the smoothing is essentially operating in a closed loop.

## V. CONCLUSIONS

In this paper, we have presented a splitting scheme for GAF, based on the method of augmented Lagrangians. The optimization takes place in three alternating steps. In the first problem, the data-term is optimized using a fixed-point scheme derived from a semi-implicit gradient-descent discretization. The second task optimizes with respect to the smoothing-term, initially by exactly solving a sparse linear system, a method we call *exact-inverse FastGAF*. Then, we substitute with an approximate inversion within the semi-implicit smoothing step, using a few fast Jacobi iterations only, to obtain the *approximate-inverse FastGAF* scheme. The third step consists in the update of the Lagrangian multipliers by integration of the residuals between the split deformation field copies. This scheme results in a considerable speedup of the registration process with respect to the baseline GAF as introduced in [11], and also compares favorably to the Demons registration method. While we describe promising solvers for those subproblems, note that those can still be improved, which will be investigated in future work. The Jacobi scheme already provides a nice speedup, but more recent and efficient methods e.g., additive operator splitting (AOS) may further improve performance [44], [36], [45], [46].

From a more fundamental perspective, geodesic active fields can be considered a generalization of the Demons method

in several respects. First, the GAF framework is designed to work on Riemannian manifolds and is thus not restricted to Euclidean images. Although Demons can be generalized to non-flat images as well, e.g. [47], on non-Cartesian grids the speed advantages of Gaussian convolution are lost. While Demons regularization is explicitly Gaussian—it penalizes the  $L_2$ -norm of the deformation field gradient—Beltrami regularization offers a tunable interpolation between Gaussian  $L_2$  and more anisotropic, TV-norm like  $L_1$  regularization. Also, the GAF framework offers the advantage of being parametrization invariant. Finally, the GAF registration framework comes with no preferred image discrepancy measure, whereas Demons has a strong preference for the  $L_2$ -norm on the image differences (SSD). With the approximate-inverse FastGAF scheme presented in this paper, we are able to achieve those relative advantages in very competitive computation times.

Finally, we have shown in multiple comparisons with publicly available state-of-the-art image registration and optical flow methods [1], [2], [3] that, considering the broad spectrum of registration tasks (stereo vision depth recovery, small displacement optical flow, large displacement medical image registration), the proposed FastGAF algorithm performs consistently well. State-of-the-art methods exceed it slightly in the individual tasks, however, FastGAF is the only method which provides consistently good results in all tasks.

## REFERENCES

- [1] D. Sun, S. Roth, and M. J. Black, “Secrets of optical flow estimation and their principles,” in *2010 IEEE Computer Society Conference on Computer Vision and Pattern Recognition*. IEEE, Jun. 2010, pp. 2432–2439.
- [2] B. Glocker, N. Komodakis, G. Tziritas, N. Navab, and N. Paragios, “Dense image registration through MRFs and efficient linear programming,” *Medical Image Analysis*, vol. 12, no. 6, pp. 731–41, Dec. 2008.
- [3] T. Brox and J. Malik, “Large displacement optical flow: descriptor matching in variational motion estimation,” *IEEE Transactions on Pattern Analysis and Machine Intelligence*, vol. 33, no. 3, pp. 500–13, Mar. 2011.
- [4] L. G. Brown, “A survey of image registration techniques,” *ACM Comput. Surveys*, vol. 24, no. 4, pp. 325–376, Dec. 1992.
- [5] J. B. A. Maintz and M. A. Viergever, “A survey of medical image registration,” *Med. Image Anal.*, vol. 2, no. 1, pp. 1–36, Mar. 1998.
- [6] M. A. Audette, F. P. Ferrie, and T. M. Peters, “An algorithmic overview of surface registration techniques for medical imaging,” *Med. Image Anal.*, vol. 4, no. 3, pp. 201–217, 2000.
- [7] B. Zitová, J. Flusser, and B. Zitova, “Image registration methods: a survey,” *Image and Vision Computing*, vol. 21, no. 11, pp. 977–1000, Oct. 2003.
- [8] M. Holden, “A Review of Geometric Transformations for Nonrigid Body Registration,” *IEEE Transactions on Medical Imaging*, vol. 27, no. 1, pp. 111–128, Jan. 2008.
- [9] G. Hermosillo, C. Chefd’hotel, and O. Faugeras, “Variational Methods for Multimodal Image Matching,” *International Journal of Computer Vision*, vol. 50, no. 3, pp. 329–343, 2002.
- [10] J.-P. Thiran, “Image matching as a diffusion process: an analogy with Maxwell’s demons,” *Medical Image Analysis*, vol. 2, no. 3, pp. 243–260, Sep. 1998.
- [11] D. Zosso, X. Bresson, and J.-P. Thiran, “Geodesic Active Fields-A Geometric Framework for Image Registration,” *IEEE Transactions on Image Processing*, vol. 20, no. 5, pp. 1300–1312, May 2011.
- [12] A. M. Polyakov, “Quantum geometry of bosonic strings,” *Phys. Lett. B*, vol. 103, no. 3, pp. 207–210, 1981.
- [13] V. Caselles, R. Kimmel, and G. Sapiro, “Geodesic Active Contours,” *Int. J. Comput. Vis.*, vol. 22, no. 1, pp. 61–79, 1997.
- [14] R. Glowinski and P. Le Tallec, *Augmented Lagrangian and operator-splitting methods in nonlinear mechanics*. Philadelphia: Society for Industrial and Applied Mathematics (SIAM), Jan. 1989.

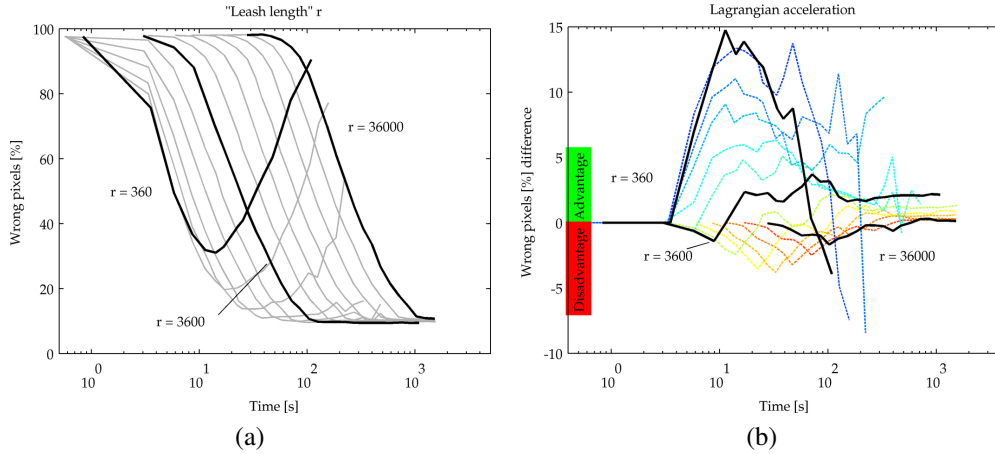


Fig. 5: Influence of the penalty term and the Lagrangian multiplier on the registration performance. (a) Smaller  $r$  increases the learning rate, i.e. the step length, at the cost of stability due to a too big data step (supra-critical step-length). Above a certain level, once stability achieved, increasing  $r$  only scales the computation time without gaining in precision (sub-critical step-length). (b) Compared to penalty-term only, the Lagrangian multiplier has a favorable impact. In particular around the critical step-length, the registration outcome is significantly improved, while farther away in the sub-critical zone, the impact is less pronounced.

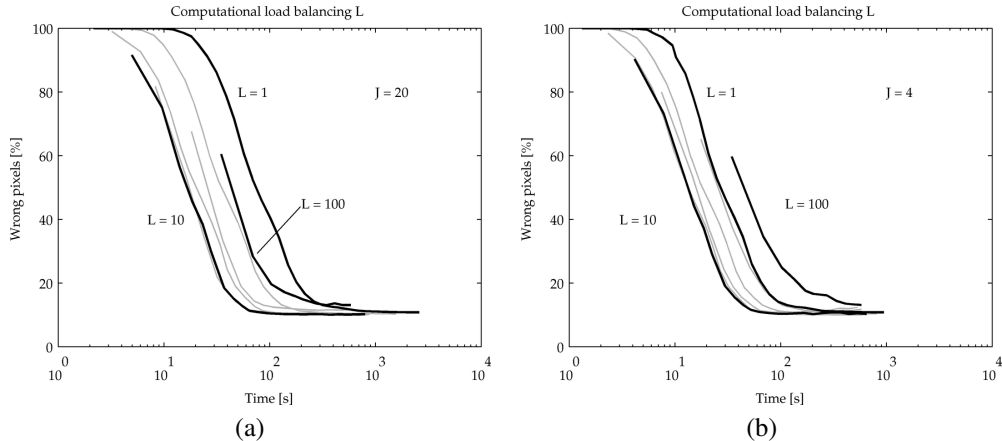


Fig. 6: Computational load balancing  $L$ . Subdividing the data-step allows reducing  $r$  by  $L$  while roughly keeping the same data-stability. This can provide speedups, as in effect a smoothing step (and Lagrangian update) is only performed after  $L$  data steps. Relatively small load balancing factors, here about  $L = 10$  yields best performance. Beyond, e.g., at  $L = 100$ , the speed gain becomes negligible while the regularization step is performed too seldom and registration quality is decreased. (a) The speedup is important for computationally heavy smoothing task  $J = 20$  (or exact inverse). (b) For lightweight smoothing,  $J = 4$ , the speed gains are less pronounced.

- [15] P. L. Lions and B. Mercier, "Splitting Algorithms for the Sum of Two Nonlinear Operators," *SIAM J. Numer. Anal.*, vol. 16, no. 6, pp. 964–979, Dec. 1979.
- [16] J. Nocedal and S. J. Wright, *Numerical optimization*, 2nd ed. Springer, Berlin, 2006.
- [17] P. Hellier, C. Barillot, I. Corouge, B. Gibaud, G. Le Goualher, D. L. Collins, A. Evans, G. Malandain, N. Ayache, G. E. Christensen, and H. J. Johnson, "Retrospective evaluation of intersubject brain registration," *IEEE Transactions on Medical Imaging*, vol. 22, no. 9, pp. 1120–1130, Sep. 2003.
- [18] T. Vercauteren, X. Pennec, A. Perchant, and N. Ayache, "Diffeomorphic demons: Efficient non-parametric image registration," *Neuroimage*, vol. 45, no. 1, Supplement 1, pp. S61–S72, Mar. 2009.
- [19] J.-M. Peyrat, H. Delingette, M. Serresant, C. Xu, and N. Ayache, "Registration of 4D cardiac CT sequences under trajectory constraints with multichannel diffeomorphic demons," *IEEE Transactions on Medical Imaging*, vol. 29, no. 7, pp. 1351–68, Jul. 2010.
- [20] H. Jia, G. Wu, Q. Wang, and D. Shen, "ABSORB: Atlas Building by Self-organized Registration and Bundling," *NeuroImage*, vol. 51, no. 3, pp. 1057–70, Jul. 2010.
- [21] B. B. Avants, N. J. Tustison, G. Song, P. A. Cook, A. Klein, and J. C. Gee, "A reproducible evaluation of ANTs similarity metric performance in brain image registration," *NeuroImage*, vol. 54, no. 3, pp. 2033–44, Feb. 2011.
- [22] B. Dong, Y. J. Graves, X. Jia, and S. B. Jiang, "Optimal Surface Marker Locations for Tumor Motion Estimation in Lung Cancer Radiotherapy," Apr. 2012. [Online]. Available: <http://arxiv.org/abs/1204.4719>
- [23] Y. Zhang, D. Boye, C. Tanner, A. J. Lomax, and A. Knopf, "Respiratory liver motion estimation and its effect on scanned proton beam therapy," *Physics in medicine and biology*, vol. 57, no. 7, pp. 1779–95, Apr. 2012.
- [24] K. Schulze, K. Mueller, and S. Koelsch, "Auditory stroop and absolute pitch: An fMRI study," *Human brain mapping*, Feb. 2012.
- [25] P. Muyan-Ozcelik, J. D. Owens, J. Xia, and S. S. Samant, "Fast Deformable Registration on the GPU: A CUDA Implementation of

- Demons,” in *2008 International Conference on Computational Sciences and Its Applications*. IEEE, Jun. 2008, pp. 223–233.
- [26] X. Gu, H. Pan, Y. Liang, R. Castillo, D. Yang, D. Choi, E. Castillo, A. Majumdar, T. Guerrero, and S. B. Jiang, “Implementation and evaluation of various demons deformable image registration algorithms on a GPU,” *Physics in medicine and biology*, vol. 55, no. 1, pp. 207–19, Jan. 2010.
- [27] X. Zhen, X. Gu, H. Yan, L. Zhou, X. Jia, and S. B. Jiang, “CT to Cone-beam CT Deformable Registration With Simultaneous Intensity Correction,” Apr. 2012. [Online]. Available: <http://arxiv.org/abs/1204.6295>
- [28] N. Sochen, R. Kimmel, and R. Malladi, “A general framework for low level vision,” *IEEE Transactions on Image Processing*, vol. 7, no. 3, pp. 310–318, 1998.
- [29] X. Bresson, P. Vandergheynst, and J.-P. Thiran, “Multiscale Active Contours,” *Int. J. Comput. Vis.*, vol. 70, no. 3, pp. 197–211, 2006.
- [30] A. W. Toga, *Brain Warping*. Academic Press, 1999.
- [31] D. Zosso, X. Bresson, and J.-P. Thiran, “Geodesic Active Fields - A Geometric Framework for Image Registration,” Ecole Polytechnique Fédérale de Lausanne (EPFL), Tech. Rep. LTS-REPORT-2010-001, 2010.
- [32] D. P. Bertsekas, “Multiplier methods: A survey,” *Automatica*, vol. 12, no. 2, pp. 133–145, 1976.
- [33] T. Goldstein and S. Osher, “The Split Bregman Method for L1-Regularized Problems,” *SIAM J. Imaging Sci.*, vol. 2, no. 2, pp. 323–343, Jan. 2009.
- [34] X.-C. Tai and C. Wu, “Augmented Lagrangian Method, Dual Methods and Split Bregman Iteration for ROF Model,” in *Scale Space and Variational Methods in Computer Vision*, ser. Lecture Notes in Computer Science, vol. 5567. Berlin, Heidelberg: Springer, 2009, pp. 502–513.
- [35] R. Ben-Ari and N. Sochen, “A geometric framework and a new criterion in optical flow modeling,” *J. Math. Imaging Vis.*, vol. 33, no. 2, pp. 178–194, Feb. 2009.
- [36] J. Weickert, B. M. ter Haar Romeny, and M. A. Viergever, “Efficient and reliable schemes for nonlinear diffusion filtering,” *IEEE Transactions on Image Processing*, vol. 7, no. 3, pp. 398–410, Mar. 1998.
- [37] D. B. Duncan and M. A. M. Lynch, “Jacobi Iteration in Implicit Difference Schemes for the Wave Equation,” *SIAM J. Numer. Anal.*, vol. 28, no. 6, pp. 1661–1679, Dec. 1991.
- [38] J. L. Barron, D. J. Fleet, and S. S. Beauchemin, “Performance of optical flow techniques,” *International Journal of Computer Vision*, vol. 12, no. 1, pp. 43–77, Feb. 1994.
- [39] D. Scharstein and R. Szeliski, “A taxonomy and evaluation of dense two-frame stereo correspondence algorithms,” *Int. J. Comput. Vis.*, vol. 47, no. 1, pp. 7–42, 2002.
- [40] I. Tosic, I. Bogdanova, P. Frossard, and P. Vandergheynst, “Multiresolution motion estimation for omnidirectional images,” in *Proceedings of 13th EUSIPCO*, 2005.
- [41] C. Geyer and K. Daniilidis, “A Unifying Theory for Central Panoramic Systems and Practical Implications,” in *Computer Vision ECCV 2000*, ser. Lecture Notes in Computer Science. Berlin, Heidelberg: Springer, 2000, vol. 1843, ch. 29, pp. 445–461.
- [42] ——, “Catadioptric Projective Geometry,” *Int. J. Comput. Vis.*, vol. 45, no. 3, pp. 223–243, Dec. 2001.
- [43] I. Bogdanova, X. Bresson, J.-P. Thiran, and P. Vandergheynst, “Scale space analysis and active contours for omnidirectional images,” *IEEE Transactions on Image Processing*, vol. 16, no. 7, pp. 1888–1901, Jul. 2007.
- [44] J. Weickert, “A review of nonlinear diffusion filtering,” in *Scale-space theory in computer vision*, ser. Lecture Notes in Computer Science, vol. 1252. Berlin, Germany: Springer-Verlag, 1997, pp. 3–27.
- [45] R. Malladi and I. Ravve, “Fast Difference Schemes for Edge Enhancing Beltrami Flow,” in *ECCV 2002*, ser. Lecture Notes in Computer Science, vol. 2350, 2002, pp. 343–357.
- [46] L. Dascal, G. Rosman, X.-C. Tai, and R. Kimmel, “On Semi-implicit Splitting Schemes for the Beltrami Color Flow,” in *Scale Space and Variational Methods in Computer Vision*, ser. Lecture Notes in Computer Science, vol. 5567. Springer Berlin / Heidelberg, 2009, pp. 259–270.
- [47] B. T. T. Yeo, M. R. Sabuncu, T. Vercauteren, N. Ayache, B. Fischl, and P. Golland, “Spherical Demons: Fast Diffeomorphic Landmark-Free Surface Registration,” *IEEE Transactions on Medical Imaging*, vol. 29, no. 3, pp. 650–668, Mar. 2010.



**Dominique Zosso** (S’06, M’11) received both, the MSc. degree in electrical and electronics engineering and the PhD degree from École Polytechnique Fédérale de Lausanne (EPFL), Lausanne, Switzerland, in 2006 and 2011, respectively.

He has previously worked as Researcher with the Structural Bioinformatics Group at the Swiss Institute of Bioinformatics and Biozentrum, University of Basel. In 2007–2012, he was Research and Teaching Assistant at the Signal Processing Laboratory at EPFL, Lausanne, Switzerland. Dr. Zosso now is a Postdoctoral Scholar in the Department of Mathematics at the University of California, Los Angeles (UCLA), with Luminita Vese, Andrea Bertozzi and Stan Osher. His current research interests include PDE and variational models for inverse problems in image processing and computer vision, and efficient algorithms to solve them.



**Xavier Bresson** received a B.A. degree in theoretical physics in 1998, a M.Sc. degree in electrical engineering from Ecole Supérieure d’Électricité, Paris, and a M.Sc. degree in signal processing from University of Paris XI in 2000. In 2005, he completed a PhD degree in the field of computer vision at École Polytechnique Fédérale de Lausanne (EPFL), Lausanne, Switzerland.

In 2006–2010, he was a Postdoc scholar in the Department of Mathematics at University of California, Los Angeles (UCLA) with Tony Chan and Stanley Osher. In 2010, he joined the Department of Computer Science at City University of Hong Kong as assistant professor. His current research works are focused on continuous convex relaxation techniques to find global solutions of non-convex problems in image processing and graph-based problems in machine learning, and a unified geometric framework for energy minimization models in image processing.

Dr. Bresson has published 39 papers in international journals and conferences.



**Jean-Philippe Thiran** (S’91–M’98–SM’03) was born in Namur, Belgium, in August 1970. He received the Electrical Engineering degree and the PhD degree from the Université catholique de Louvain (UCL), Louvain-la-Neuve, Belgium, in 1993 and 1997, respectively. Dr Jean-Philippe Thiran joined the Swiss Federal Institute of Technology (EPFL), Lausanne, Switzerland, in February 1998 as a senior lecturer. From 2004 to 2011 he was an Assistant Professor (tenure track), responsible for the image analysis group (LTS5). In 2011 Dr Thiran has

been promoted to Associate Professor in Signal Processing at EPFL. He also holds a 20% associate professor position with the Department of Radiology of the University Hospital Center and University of Lausanne (CHUV-UNIL).

Dr. Thiran’s current scientific interests include image segmentation, analysis and multimodal signal processing, with application to medical imaging, remote sensing, face image analysis and human-computer interaction.

Prof. Thiran is author or co-author of 9 book chapters, 100 journal papers and more than 165 peer-reviewed papers published in proceedings of international conferences. He holds 5 international patents. From 2001 to 2005 he was Co-Editor-in-Chief of the Signal Processing international journal (published by Elsevier Science). He is currently an associate editor of the IEEE Transactions on Image Processing. Among many professional duties, he was the general chairman of the 2008 European Signal Processing Conference (EUSIPCO 2008) and will be the technical co-chair of the IEEE Int. Conf. on Image Processing (ICIP) in 2015. He is a senior member of the IEEE and a member of the “Image, Video, and Multidimensional Signal Processing” (IVMSP) Technical Committee (2009–2014) of the IEEE Signal Processing Society.